DOI: 10.1002/adsc.200900089

Bismuth-Doped Ceria, $Ce_{0.90}Bi_{0.10}O_2$: A Selective and Stable Catalyst for Clean Hydrogen Combustion

Jurriaan Beckers,[a,*] Adam F. Lee,[b] and Gadi Rothenberg[a,*]

[a] Van 't Hoff Institute for Molecular Sciences, University of Amsterdam, Nieuwe Achtergracht 166, 1018 WV Amsterdam, The Netherlands
Fax: (+31)-20-525-5604; e-mail: J.Beckers@uva.nl or G.Rothenberg@uva.nl
[b] Department of Chemistry, University of York, York, YO10 5DD, U.K.

Received: February 10, 2009; Revised: May 18, 2009

Abstract: Bismuth-doped cerias are successfully applied as solid "oxygen reservoirs" in the oxidative dehydrogenation of propane. The lattice oxygen of the ceria is used to selectively combust hydrogen from the dehydrogenation mixture at 550 °C. This process has three key advantages: it shifts the dehydrogenation equilibrium to the desired products side, generates heat, aiding the endothermic dehydrogenation, and simplifies product separation (water *vs.* hydrogen). Furthermore, the process is safer, since it uses the catalyst's lattice oxygen instead of gaseous oxygen. We show here that bismuth-doped cerias are highly active and stable towards hydrogen combustion, and explore four different approaches for optimising their application in the oxidative dehydrogenation of propane: first, the addition of extra hydrogen which lowers hydrocarbon conversion by suppressing both combustion and coking; second, the addition of tin which completely inhibits coking; third, the addition of platinum which increases selectivity, but at the expense of lower activity. The best results are obtained through tuning the reaction temperature. At 400 °C, high activity and selectivity were obtained for the bismuth-doped ceria $Ce_{0.90}Bi_{0.10}O_2$. Here, 90% of the hydrogen feed is converted at 98% selectivity. This optimal reaction temperature can be rationalised from the hydrogen and propene temperature-programmed reduction (TPR) profiles: 400 °C lies *above* the reduction maximum of hydrogen, yet *below* that of propene. That is, this temperature is sufficiently high to facilitate rapid hydrogen combustion, but low enough to prevent hydrocarbon conversion.

Keywords: bismuth; ceria (CeO_2); doping; oxidative dehydrogenation (ODH); selective oxidation; temperature-programmed reduction (TPR)

Introduction

Bismuth, although less common than metals such as lead, copper and iron, is widely used in everyday life. Bismuth subsalicylate, for example, is the active ingredient of over-the-counter drugs such as "Bismatrol" and "Pepto-Bismol," used for treating several gastrointestinal ailments.[1] The low melting point of many bismuth alloys enables their use in sprinkler system heads, where the melting of the alloy unplugs the sprinkler,[2] and as a replacement for lead in low-temperature solders.[3] In catalysis, bismuth salts are applied as 'green catalysts' in various organic syntheses.[4–6] Bismuth is also part of a mixed-oxide catalyst used for the industrial production of acrylonitrile (the so-called "SOHIO process"), and can be used for the oxidative conversion of methane to higher hydrocarbons.[7–9] The high oxygen conductivity of bismuth oxides enables their use as electrodes for solid oxide fuel cells, or as low-temperature oxygen-permeable membranes.[10–14] These membranes can also be applied as catalysts in selective oxidations, such as the oxidation of propene.[15,16] The *BiMeVOX* mixed oxides ($Bi_4V_2O_{11}$, where part of the vanadium atoms can be replaced with a variety of metals), are a well known example.[14]

In the 1990s, supported bismuth oxides have been applied as catalysts in oxidative dehydrogenation (ODH).[17,18] Propane ODH yields valuable propene, the building block of polypropene. The demand for propene is huge, and is expected to rise to 80 million tonnes in 2010 worldwide.[19–21] Currently, crackers and oil refineries account for about 95% of the propene supply, but more advantageous methods such as metathesis and catalytic dehydrogenation of propane are gaining ground. These allow for on-demand production of high purity monomer.[22–24] Propane ODH is typically performed over supported vanadium and molybdenum oxide catalysts, with a small amount of oxygen added to the gas feed.[25,26] However, the

mixing of hydrocarbons and gaseous oxygen at elevated temperatures is potentially hazardous and limits selectivity.[25,27] These drawbacks can be overcome using a redox process, where the dehydrogenation is combined with selective hydrogen combustion.[18,28–34] The dehydrogenation is performed over conventional Pt-Sn or Cr catalysts (typically at 550–600 °C), with a 'solid oxygen reservoir' (SOR) added. The latter selectively burns the H_2 *in situ*, using its lattice oxygen (Scheme 1, *top*).[28,29] This combustion generates heat, aiding the endothermic dehydrogenation. It also shifts the equilibrium to the products side. Following the reduction of the SOR lattice, the oxygen vacancies are recharged with air, creating a cyclic redox process. Using two catalysts allows for separate tuning of the dehydrogenation and the selective hydrogen combustion. Scheme 1 (*bottom*) illustrates a possible industrial redox dehydrogenation process. Alternative process designs include recycling of material through an acceptor and a regenerator, similar to the fluid catalytic cracking process, or using a two-stage fluidised bed. Here, one would inject oxygen at the bottom of the bed and propane halfway up in the bed.

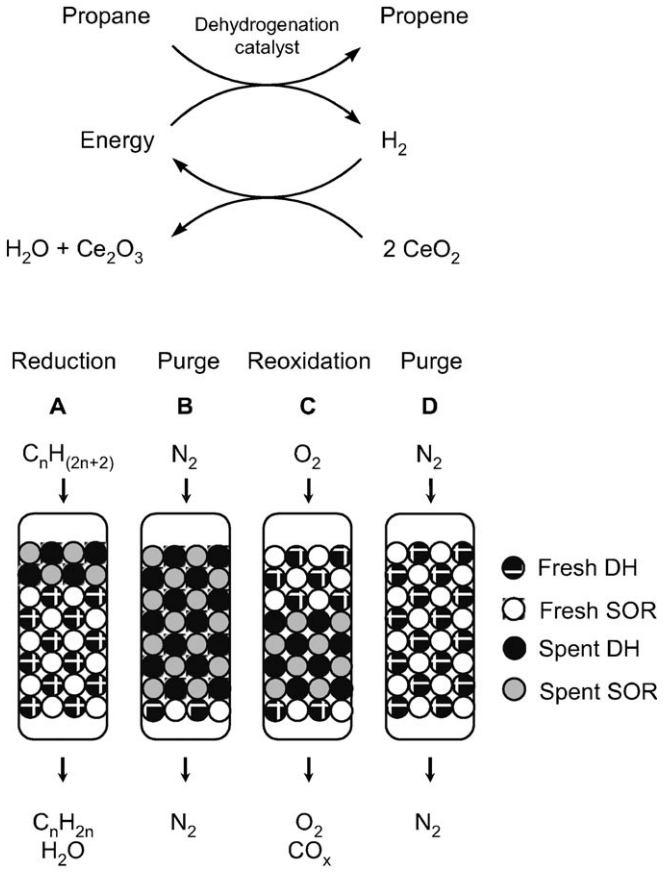

Scheme 1. *Top*: combined propane dehydrogenation and selective hydrogen combustion: the selective hydrogen combustion consumes part of the hydrogen formed during the dehydrogenation step, shifting the equilibrium to the products side and generating heat. *Bottom*: cartoon of the complete redox cycle. After the dehydrogenation step **A**, the bed is flushed with nitrogen (**B**), and the catalysts are regenerated through reoxidation (**C**). This burns coke from the dehydrogenation catalyst and restores the lattice oxygen of the SOR catalyst. After another nitrogen flush (**D**), the reactor is ready for the next redox cycle.

Supported metal oxides, such as bismuth oxide, have been applied as SOR, exhibiting high selectivity towards hydrogen combustion. However, due to their low melting points they are unstable under redox cycling.[29,35,36] We recently discovered a new type of SOR, based on ceria, that overcomes this limitation.[37,38] Ceria is often used in redox reactions because of the facile $Ce^{3+} \leftrightarrow Ce^{4+} + e^-$ redox cycle.[39] Although it possess greater stability, the activity and selectivity of pure ceria are low.[38] Nevertheless, active and selective SOR catalysts can be formed by replacing about 10 mol% of the cerium atoms.[40,41]

In 2003, we tested ten catalysts for their selectivity towards hydrogen combustion from a mix with ethane and ethene, discovering that $Ce_{0.9}W_{0.1}O_2$ showed excellent selectivity and stability.[37] Subsequently, we employed genetic algorithms to screen and "breed" doped ceria catalysts for hydrogen combustion from a mix with propane and propene.[40] Twenty-six different dopants were used, at five possible concentrations, with a maximum of two dopants per catalyst. We found that the most promising dopants are Cu, Mn, K, Cr, Pb, Sn and Bi, with selectivities ranging from 80–98%.[41,42] Of the set of promising dopants, the highest activities were obtained using Pb and Bi. The activity is very important for practical application, since it governs the reactor volume (the amount of SOR needed) and the process cycle time. Unlike lead, bismuth has a low toxicity, and is more stable. The bismuth-doped ceria catalysts, however, are also less selective. Here, we describe several methods for increasing the selectivity of bismuth-doped ceria in selective hydrogen combustion. Furthermore, we evaluate their catalytic properties at a range of temperatures and gas compositions. The catalytic tests are complemented with extensive characterisation, including XPS surface analysis, temperature programmed reaction (TPR) studies of the interaction of the catalyst with both hydrogen and propene, and an assessment of the level of hydrocarbon coking and combustion, in relation to the catalyst composition.

Results and Discussion

Catalyst Preparation and Characterisation

All catalysts were prepared by co-melting mixtures of the metal nitrate hydrate precursors (chlorides in the cases of Pt and Sn), at 140 °C in a vacuum oven. After the precursor had liquefied, the pressure was lowered

Table 1. Catalyst characterisation and catalytic performance data at 550 °C.

Catalyst/Composition	Crystallite size [nm][a]	Lattice spacing [Å]	Selectivity [%][b]	Activity [% H_2 combusted]	Coking [mg C/10 min][c]	Combustion [vol% CO_2/10 min][d]
1/CeO_2	22	5.411	0	0	0.09	1.3
2/$Ce_{0.98}Bi_{0.02}O_2$	18	5.411	94	10	0.19	2.3
3/$Ce_{0.93}Bi_{0.07}O_2$	17	5.416	82	26	0.22	3.5
4/$Ce_{0.90}Bi_{0.10}O_2$	18	5.416	77	33	0.16	4.0
5/$Ce_{0.88}Bi_{0.08}Sn_{0.04}O_2$	14	5.412	82	45	0.00	4.7
6/$Ce_{0.98}Sn_{0.02}O_2$	12	5.408	77	8	0.10	2.8
7/$Ce_{0.93}Sn_{0.07}O_2$	10	5.407	89	20	0.00	4.2
8/$Ce_{0.91}Bi_{0.05}Pt_{0.04}O_2$/Pt(0)[e]	12	5.417	95	14	0.10	5.9
9/$Ce_{0.98}Pt_{0.02}O_2$	16	5.411	0	0	0.77	2.3

[a] Derived from the peak broadening of the Ce(111) XRD peak using the Scherrer equation.
[b] The first data point (after 25 s), is not taken into account when calculating selectivity, since all catalysts show unselective combustion here, probably due to unselective reaction with adsorbed oxygen.
[c] The level of coking is determined from the amount of CO and CO_2 detected by MS during the reoxidation cycle. It therefore represents the total amount of carbon (mg) deposited on the catalyst surface during one 10 min reduction cycle.
[d] Summation of the amount of CO_2 detected in 15 GC analysis performed during the 10 min reduction cycle. Note that most catalysts only produce CO_2 during the first 75 seconds of this cycle.
[e] XRD analysis shows that a separate metallic platinum phase is present.

and a solid mixed metal nitrate formed. This was converted into the mixed oxide by calcining in static air at 700 °C for 5 h.[42] Importantly, these catalysts were not prepared by impregnating a cerium oxide support. Rather, the co-melting of the cerium nitrate with the nitrate or chloride of the appropriate metal yields a liquid precursor. This ensures ideal mixing prior to calcination, incorporating the dopant into the fluorite lattice.

The catalyst composition, characterisation data and catalytic performance of all catalysts are given in Table 1. The selectivity is defined as:

$$\frac{conversion_{H_2}}{conversion_{H_2 + C_3H_6 + C_3H_8}} \times 100$$

with the conversion being the percentage of the hydrogen, propane or propene gas feed which is converted by the catalysts. The catalyst activity is the percentage of the hydrogen feed combusted by each catalyst. Except for **8**, the X-ray diffraction patterns of the catalysts exclusively exhibit the ceria fluorite structure (not shown), and no oxides of the added metal are observed. Catalyst **8** contains some metallic platinum. The data of Table 1 show that the crystallite size and lattice parameters do vary between the catalysts. This variation, however, is small, and we previously showed that the effect of such small variations on the selectivity, activity and stability are overruled by dopant type.[40]

Selectivity towards Hydrogen Oxidation

In a typical reaction, 250 mg of sample are placed on a quartz wool plug in a quartz reactor and heated to 550 °C in 1% v/v O_2/Ar. The catalytic activity and product selectivity are determined by GC and MS over nine redox cycles. Each cycle consists of a 10 min reduction step in 4:1:1% v/v C_3H_8:C_3H_6:H_2 in Ar, and an 18 min oxidation step in 1% v/v O_2/Ar, separated by 4 min purge cycles. The 4:1:1 ratio of the reductive gases simulates the effluent stream from industrial propane dehydrogenation.[18] Figure 1 shows the reaction profile of catalyst **3** ($Ce_{0.93}Bi_{0.07}O_2$), which

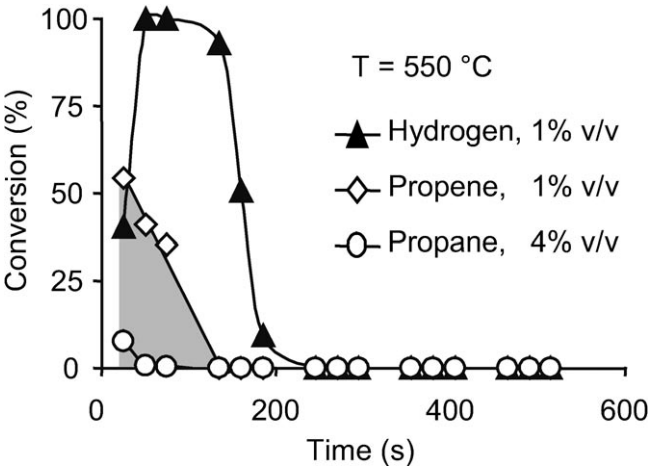

Figure 1. Reaction profile of $Ce_{0.93}Bi_{0.07}O_2$ (**3**) at 550 °C, showing the H_2 (▲), C_3H_8 (○) and C_3H_6 (◇) conversion during a reduction cycle. The grey area indicates the level of propene conversion.

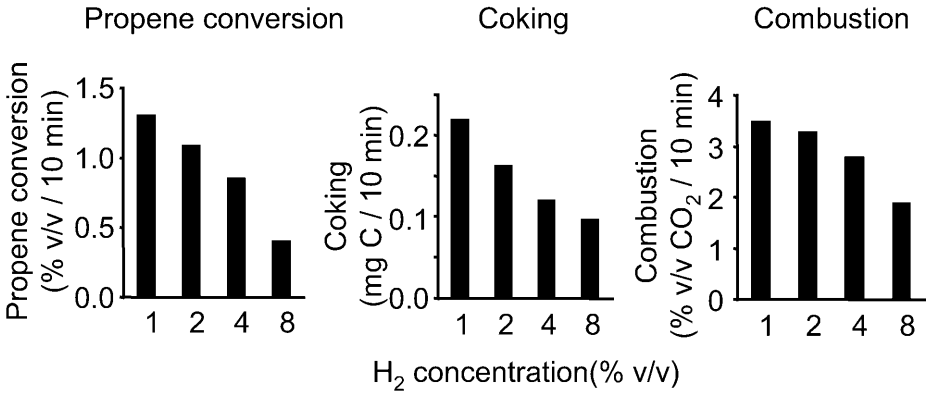

Figure 2. Propene conversion, coking and hydrocarbon combustion at various hydrogen concentrations using $Ce_{0.93}Bi_{0.07}O_2$ (**3**) (550 °C, 1% v/v propene and 4% v/v propane). Note: all measurements were performed on one sample. To check if the subsequent measurements have not affected the sample, the measurement at 1% H_2 was repeated, and gave similar results to the first measurement. The coking data pertains to the total amount of carbon (mg), which is deposited on the catalyst surface during a single reduction cycle. The combustion data is a summation of the amount of CO_2 detected in 15 GC analyses performed during the 10 min reduction cycle. Note that most catalysts only produce CO_2 during the first 75 seconds of this cycle.

is typical for bismuth-doped ceria catalysts (**2**, **3**, **4**, Table 1). Figure 1 shows the conversions of hydrogen (▲), propene (◇) and propane (○), during the reduction cycle. The Ce-Bi-O catalysts have a good activity towards hydrogen combustion. Indeed, from a set of 61 doped ceria catalysts, containing 26 different dopant elements, the Bi-doped catalysts were amongst the most active, second only to lead-doped ceria.[38,40] Lead, however, easily segregates from the ceria, forming a separate lead oxide phase, which is unstable under redox cycling.[35] The Bi-doped cerias are more stable, but convert part of the propene feed (grey area in Figure 1). Thus, having discovered that the bismuth-doped ceria is an active, stable and non-toxic SOR catalyst, we set out to improve its selectivity.

Increasing the Hydrogen Concentration

Studies in hydroprocessing of light gas oil showed that an increased concentration of hydrogen can limit coking, possibly by shielding the catalyst surface from hydrocarbons.[43] To check whether this also holds for our doped cerias, we assessed the level of propene conversion of catalyst **3** ($Ce_{0.93}Bi_{0.07}O_2$) at 1–8% v/v of H_2 (the equilibrium mixture of the dehydrogenation contains 1% v/v of H_2, 1% v/v C_3H_6 and 4% v/v C_3H_8).[44] Figure 2 shows that indeed propene conversion, coking, and hydrocarbon combustion are all lower at higher H_2 concentrations.[45] This strategy, however, is not advantageous in the selective hydrogen combustion, since adding hydrogen shifts the equilibrium towards the reactants side (see Scheme 1).

Addition of Tin

Tin is an essential promoter in the Pt-based dehydrogenation catalysts, since it limits catalyst deactivation due to coking.[46] We found that it has the same beneficial effect when applied as a dopant in the ceria SOR catalysts. Tin is the only element, out of 25 tested, that prevents coking.[40] Figure 3 shows the level of coking of plain ceria (**1**, reference catalyst), the Bi-doped catalysts **2**–**4** and $Ce_{0.88}Bi_{0.08}Sn_{0.04}O_2$ (**5**). We have seen that both the activity and the level of hydrocarbon combustion increase with increasing Bi-doping (catalysts **2**–**4**, Table 1). However, the amount of coking is not correlated to the amount of bismuth dopant, yet it is higher compared to plain ceria. This

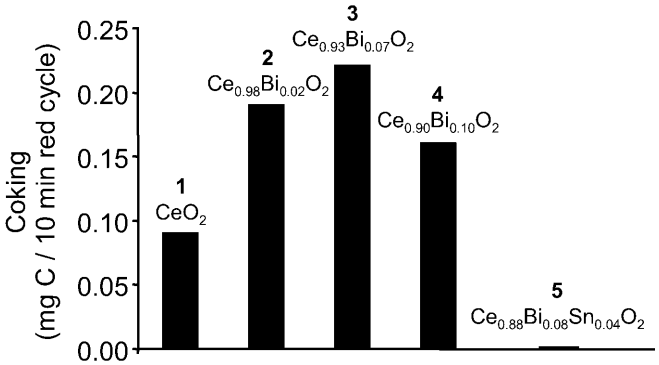

Figure 3. Effect of Bi concentration and Sn addition on coking. Ceria is added as a reference. The data reflect the total amount of carbon which is deposited on the catalyst surface during one 10 min reduction cycle. The coking level of catalyst **5** is zero.

coking is completely inhibited by adding 4 mol% of tin (**5**, Table 1). At too low doping levels, coking is not prevented (**6**, **7**, Table 1). Possibly, the 2 mol% tin cannot cover all of the surface. Since tin itself is active in the selective hydrogen combustion (**6**, **7**), the activity of the bismuth catalyst is increased upon addition of tin.

Catalysts **3** and **5** contain roughly equal amounts of Bi, but adding 4 mol% of tin to catalyst **5** increases its activity by about 40%. Tin also increases hydrocarbon conversion *via* combustion. That is, tin increases the activity and limits coking, but does not increase the total selectivity of the catalysts. Note that the Bi concentration also affects the selectivity. The low loaded catalyst **2** ($Ce_{0.98}Bi_{0.02}O_2$) is more selective than **3** and **4**, since the propene conversion drops quicker than the hydrogen conversion (Table 1). These low doping levels, however, also result in a drop in activity.

Addition of Platinum

Doping ceria with noble metals such as Pt, Pd and Ru results in unselective catalysts, with high levels of coking and cracking of the hydrocarbons.[38,40,42] Surprisingly, this is not the case for the Pt-Bi doped ceria **8**.[47] Figure 4 shows the reaction profiles of catalyst **8** and catalyst **9**, $Ce_{0.98}Pt_{0.02}O_2$. The reaction profile of **9** is typical for noble metal-doped cerias, showing high levels of hydrocarbon conversion, and *formation* of hydrogen (a negative conversion), as a result of coking. Figure 4 shows that the Pt-Bi doped **8** is much more selective. Surprisingly, propene conversion over catalyst **8** is also limited to the first 25 s of the reduction cycle, unlike the typical long-term propene conversion seen for Bi-doped cerias (see Figure 1). The initial propane and propene conversions of **8** are still higher, however, than those of Bi-doped ceria (compare Figure 4 with Figure 1). Since these unselective reactions also use up oxygen, the activity of the Pt-Bi-doped **8** is lower than that expected from its Bi content (compare with the Bi-doped catalysts **2**–**4**). Still, the selectivity of the Pt-Bi-doped ceria **8** is dramatically higher than any Pt-doped ceria catalyst tested (11 in total).[40] Indeed, alumina-supported Pt is used in dehydrogenation catalysts, but Sn needs be added to limit coking.[48] Our results show that adding bismuth can have the same effect.

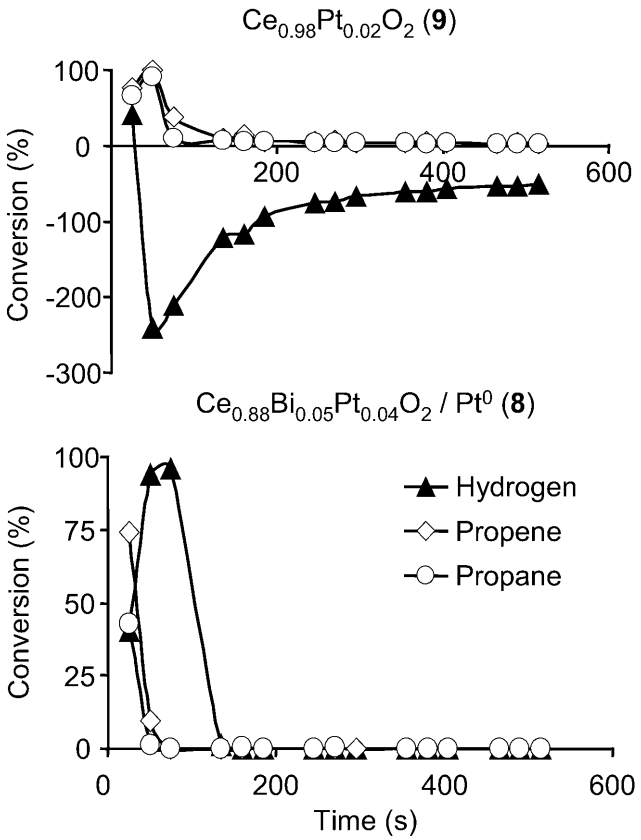

Figure 4. Reaction profiles of $Ce_{0.98}Pt_{0.02}O_2$ (**9**, *top*) and $Ce_{0.91}Bi_{0.05}Pt_{0.04}O_2$, (**8**, *bottom*), showing the H_2 (▲), C_3H_8 (○) and C_3H_6 (◇) conversion during a reduction cycle. Note: for catalyst **8**, some hydrogen formation is observed in the last part of the reduction cycle.

Table 2 shows the surface concentrations and binding energies of catalysts **3** (Ce-Bi-O), **9** (Ce-Pt-O), and **8** (Ce-Bi-Pt-O), as determined by XPS.[49] The surface concentrations of the dopants are lower than the expected bulk value (see Table 2). However, the surface concentration ratios of Bi and Pt of the three catalysts are in accordance with the bulk concentrations. Analysis of the oxidation states of the dopants

Table 2. Surface concentrations of the catalysts components as determined by XPS and binding energies of Bi and Pt.

Catalyst	Composition	Surface composition (% of total)					Binding energy (eV)	
		Ce	O	Bi	Pt	C[a]	Bi $4f_{7/2}$	Pt $4f_{7/2}$
3	$Ce_{0.93}Bi_{0.07}O_2$	22.4	55.1	4.6	–	17.8	156.4	–
9	$Ce_{0.98}Pt_{0.02}O_2$	25.6	53.8	–	0.7	20.0	–	70.2
8	$Ce_{0.91}Bi_{0.05}Pt_{0.04}O_2$/Pt(0)	25.4	57.3	3.4	1.2	12.7	157.3	71

[a] Analysis of high resolution carbon C 1*s* spectra shows identical carbon species for all samples. The detected carbon, therefore, most likely stems from a common contaminant and not from specific Pt-C_xO_y or Bi-C_xO_y species. Therefore, this common contaminant will not affect the concentration ratios presented here.

shows that the bismuth is present as Bi(0) in the singly doped catalyst **3** (see Table 2). Since no bismuth metal is detected by XRD, the catalyst surface likely consists of Bi(0) clusters with a size below the XRD detection limit (< 3 nm). The same holds for the platinum-doped **9**: metallic Pt is detected by XPS, but not by XRD. Analysis of the binding energies of the Bi-Pt-doped catalyst **8** indicates that alloy formation occurs between the bismuth and platinum. There is a significant chemical shift of +0.8 eV for both Bi and Pt surface species, with the resulting bismuth binding energy in good agreement with that reported for Bi-Pt alloys.[50,51] The mutual perturbation of both dopants also shows Bi-Pt alloying. Note that the typical chemical shifts between metallic and oxidic bismuth (Bi_2O_3) are much larger, ranging from 1.4 to 4.4 eV.[52–54] Although the presence of bismuth oxide cannot be entirely excluded, the small chemical shift between catalysts **3** and **8** points to **8** containing a mixture of Bi(0) particles and Bi-Pt alloy particles, and not bismuth oxide formation.[50,51] The increased selectivity of the Bi-Pt catalyst **8** as compared to Pt-doped cerias most likely results from alloy formation, and the associated electronic (in addition to geometric) influence of bismuth upon platinum.[55]

Variation of Temperature

The selectivity of an SOR is governed by its relative reactivity towards hydrogen *versus* hydrocarbons. A selective catalyst will have a high hydrogen reduction rate, and a low hydrocarbon reduction rate at the reaction temperature (550 °C). Previously, we showed that the reduction rate at 550 °C is related to the reducibility of the catalyst, as determined by H_2-TPR.[42] Catalysts with a low TPR reduction temperature, have a high reduction rate at 550 °C. Conversely, catalysts with a high reduction temperature (close to 550 °C), have a low reduction rate at 550 °C. To understand what governs the redox cycle, we performed both hydrogen and propene TPR on selected catalysts. In a typical experiment, 250 mg of catalyst are heated from room temperature to 600 °C in either 5% v/v H_2/Ar or 1% v/v C_3H_6/Ar. The hydrogen consumption or CO_2 production is determined by MS. The CO_2 formation is chosen as a measure of the propene conversion, since the MS response for CO_2 is much higher than that for C_3H_6, and both profiles are identical. For better comparison, the hydrogen conversion is inverted. We chose propene as a measure of the SOR reactivity towards hydrocarbons, because apart from the initial unselective part, the catalysts do not convert propane below 550 °C.

Figure 5 shows the reduction profiles of pure ceria, $Ce_{0.93}Bi_{0.07}O_2$ (**3**) and $Ce_{0.92}Pb_{0.08}O_2$. Doping with Pb yields a highly selective catalyst, however, with lower

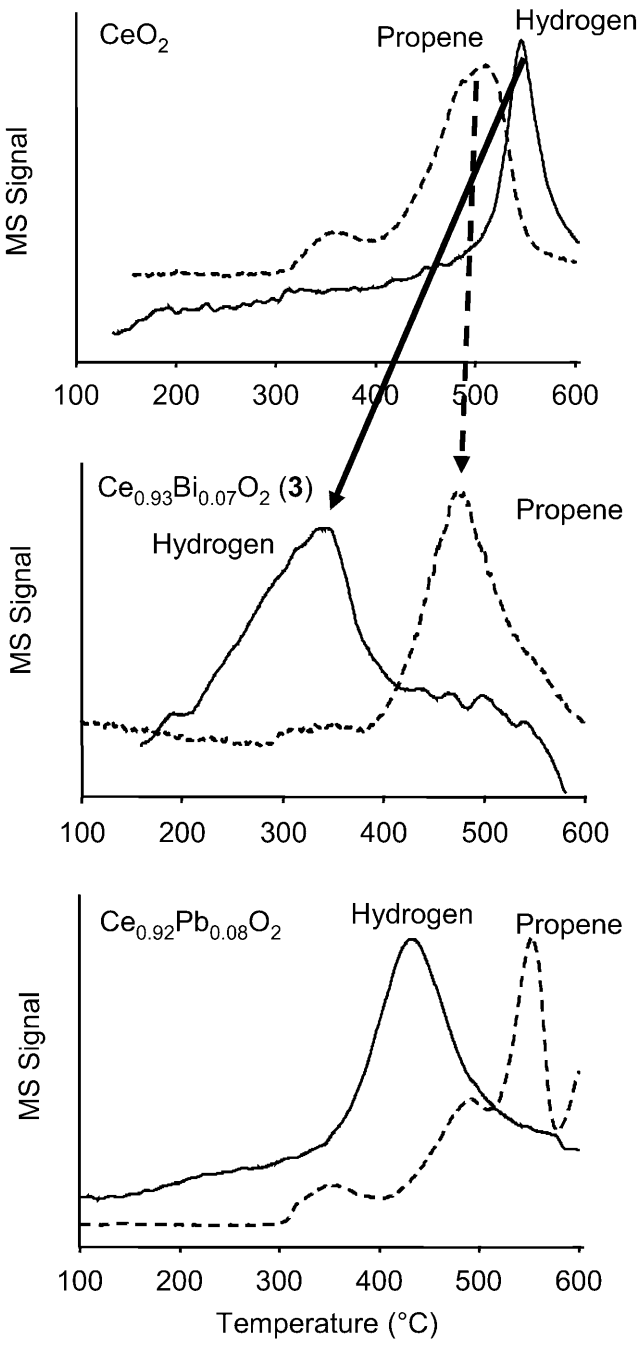

Figure 5. H_2-TPR and C_3H_6-TPR for ceria (*top*), $Ce_{0.93}Bi_{0.07}O_2$ (**3**, *middle*) and $Ce_{0.92}Pb_{0.08}O_2$ (*bottom*). Fresh samples were heated from 25 °C to 600 °C in either 5% v/v H_2/Ar or 1% v/v C_3H_6/Ar. The CO_2 evolution is taken as a measure for the propene conversion. The H_2 profile is inverted for better comparison. Note that above 550 °C, **3** shows a net *formation* of hydrogen. Hydrogen adsorption by ceria below 400 °C, and its subsequent release at higher temperatures has been reported by several other authors.[56,57] The hydrogen reduction peak of catalyst **3** between 200–400 °C is indeed caused by hydrogen combustion, since an identical water peak is observed by MS (from 400 °C onwards, no water is detected).

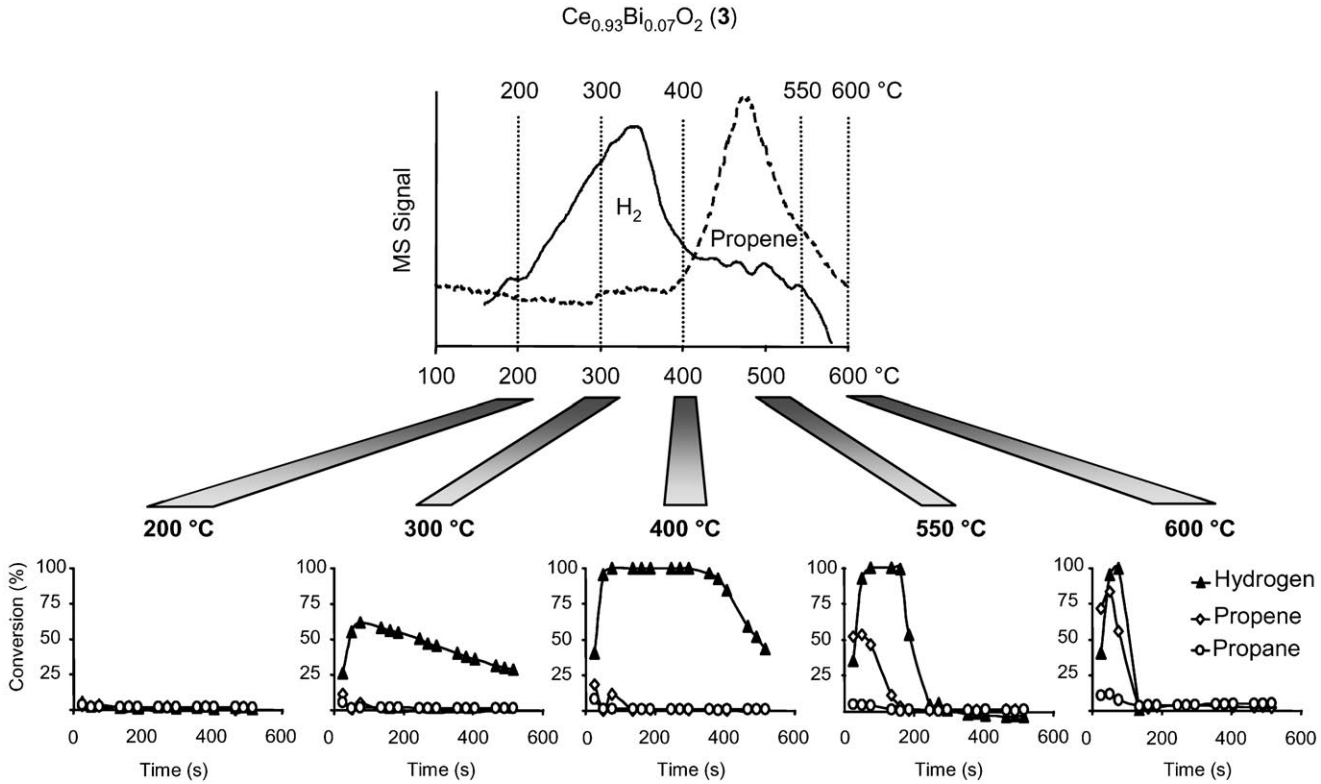

Figure 6. *Top*: H_2-TPR and propene-TPR of $Ce_{0.93}Bi_{0.07}O_2$ **3**. *Bottom*: selective hydrogen combustion data of $Ce_{0.90}Bi_{0.10}O_2$ (**4**) at various temperatures. The TPR data of **3** are shown, since a separate Bi_2O_3 phase had formed in case of catalyst **4** after the catalytic measurements at 600 °C.

stability (*vide supra*). Note that these data represent two separate experiments, where a fresh sample is reduced in either hydrogen or in propene, but not in a mixture of the two. The data show that, for the unselective CeO_2, the reduction maximum of propene occurs at lower temperatures than that of hydrogen (Figure 5, *top*). That is, this catalyst has a higher affinity for propene combustion than hydrogen combustion (the hydrocarbon combustion rate will be higher).[42] In contrast, for the selective $Ce_{0.93}Bi_{0.07}O_2$ (**3**), this order is reversed: the reduction maximum for hydrogen occurs before that of propene. Thus, hydrogen is reduced faster than propene at 550 °C, and indeed the Bi-doped catalysts are much more selective than plain ceria. Note that for the Bi-doped catalyst, the bulk reduction temperature of propene lies at 500 °C, that is, still below the reaction temperature of 550 °C. Indeed, the Bi-doped catalysts do convert part of the propene feed (see also Figure 1). The reduction maximum of hydrogen of the selective Pb-doped ceria also lies below that of propene (Figure 5, *bottom*), and for this catalyst, the bulk reduction temperature of propene is higher compared to that of the Bi-doped catalysts. Indeed, Pb-doped cerias are even more selective, albeit less stable than the Bi-doped ones.

The reduction profiles of $Ce_{0.90}Bi_{0.10}O_2$ (**4**) show that the selectivity of this catalyst may be optimised by selecting the appropriate reaction temperature. At temperatures below ~400 °C, the catalyst should be ineffective for propene combustion, but still be able to combust hydrogen, affording high selectivity. Above 400 °C, propene combustion should dominate, lowering selectivity to the desired H_2 combustion. To test this hypothesis, we ran five selective hydrogen combustion experiments at 200–600 °C (see Figure 6, Table 3). At 200 °C, TPR shows neither hydrogen or propene combustion, and the catalyst is inactive (Figure 6). At 300 °C, the H_2-TPR shows that $Ce_{0.90}Bi_{0.10}O_2$ burns hydrogen, and the catalyst is active (*bottom row*). Note this temperature is still below the hydrogen combustion maximum. At 400 °C the catalyst is more active, but still selective. At 550 °C and 600 °C, significant propene combustion and coking is visible from both the TPR and catalytic experiments (numerical data is shown in Table 3).

Conclusions

Bismuth-doped cerias (Bi concentration 2–10 mol%) have great potential as the "solid oxygen reservoir"

Table 3. Catalytic data of $Ce_{0.90}Bi_{0.10}O_2$ (**4**) at various temperatures.

Reaction temperature [°C][a]	Selectivity [%]	Activity [% H_2 combusted]	Coking [mg C/ 10 min]	Combustion [vol% CO_2/ 10 min]
200	n.a.	0	0.00	0
300	100	45	0.03	0
400	98	89	0.06	0.5
550	77	33	0.16	4.0
600	56	14	0.21	5.7

[a] All measurements were performed on the same sample, in the order 550 °C, 200 °C, 300 °C, 400 °C, 600 °C. After the 600 °C measurement, a yellow band was observed at the reactor exit, and XRD analysis of the sample showed that a separate Bi_2O_3-phase had formed.

component in a novel catalytic process for propane dehydrogenation. While hydrogen combustion activity rises with increasing Bi content from 2 to 10 mol%, this also results in higher hydrocarbon conversion. We explore four strategies to increase the selectivity and/or activity of the Ce-Bi-O catalysts. First, the addition of extra hydrogen decreases hydrocarbon conversion by suppressing both coking and combustion pathways. However, this strategy is not advantageous in a dehydrogenation process since it shifts the equilibrium towards the reactants. Second, we found that addition of 4–7 mol% tin completely inhibits hydrocarbon coking, and increases hydrogen combustion. Unfortunately tin also boosts the level of hydrocarbon combustion. Third, adding Pt increases selective H_2 combustion, but lowers net activity. The best performance is obtained by controlling the reaction temperature. The optimal temperature for Bi-doped ceria is 400 °C, wherein $Ce_{0.90}Bi_{0.10}O_2$ shows 98% selectivity and converts 90% of the hydrogen feed. Indeed for the majority of the reduction cycle, this catalyst converts all the hydrogen *without* converting any propane or propene. That is, at 400 °C, the Bi-doped catalyst does not require additional tin, platinum or extra hydrogen to achieve high selectivity and activity. The optimal reaction temperature can be rationalised from hydrogen and propene TPR measurements: 400 °C lies in between the reduction maxima for hydrogen (< 400 °C) and propene (> 400 °C), resulting in high activity and selectivity to hydrogen combustion. Similar trends were observed for $Ce_{0.92}Pb_{0.08}O_2$. For undoped ceria this phenomena is reversed: the propene reduction maximum lies *below* that for hydrogen reduction, resulting in a higher reactivity towards hydrocarbon *versus* hydrogen combustion, and is thus an unselective catalyst.

Experimental Section

Materials and Instrumentation

Chemicals were purchased from Sigma–Aldrich or Merck and used as received. Gases were purchased from Praxair and had a purity of 99.5% or higher. The O_2, He, Ar and N_2 streams were purified further over molecular sieves and/or BTS columns. Powder X-ray diffraction measurements were performed using a Philips PW-series X-ray diffractometer with a Cu tube radiation source ($\lambda = 1.54$ Å), a vertical axis goniometer and a proportional detector. The 2θ detection measurement range was 10°–93° with a 0.02° step size and a 5 second dwell time. Lattice constants and crystallite sizes were obtained after Rietveld refinement (structure fit) using PANalytical's X′pert software package. GC analysis was performed on an Interscience CompactGC equipped with TCD detectors, separating water, CO_2 and C_2 and C_3 hydrocarbons on a Porabond Q column (He carrier gas) and H_2, CO, CH_4, O_2 and N_2 on a 5 Å mol sieve column (Ar carrier gas). MS analysis was performed using a Pfeiffer QMS 200 mass spectrometer (m/z range 0–200). X-ray photoelectron spectra were recorded on a Kratos HSi spectrometer equipped with a charge neutraliser and monochromated Al K_α X-ray source (1486.61 eV) operating at 144 W. Spectra were recorded with a pass energy of 40 eV at normal emission, and energy referenced to the valence band and adventitious carbon. Analysis was conducted using CasaXPS Version 2.3.15.

Procedure for Catalyst Synthesis

The procedure for catalyst preparation was described in detail previously.[38,40] The metal nitrates (chloride in the case of Sn) are weighed in a porcelain crucible and heated to about 100 °C, so that the cerium nitrate melts. The mixture is stirred until all components are dissolved or have melted, in the case of Sn, 2–4 drops of water are added to aid the dissolution. The crucible is placed in a vacuum oven set at 140 °C and the pressure is carefully lowered to < 10 mbar (in 10–15 min), making sure no vigorous boiling occurs. After 4 h, the samples are placed in a furnace and calcined under static air at 700 °C (ramp rate 300 °C/h, 5 h hold). The resulting solid is pulverised, ground and sieved in fractions of 125–212 μm (selectivity assessment and TPR) and < 125 μm (XRD measurements).

Procedure for Testing Catalytic Activity

The activity and selectivity were determined using an automated cyclic redox reactor system built in-house, described in detail elsewhere.[38] In a typical experiment, about 250 mg of sample (125–212 μm) were placed on a quartz wool plug in a 4 mm i.d. quartz reactor. The reactor was placed in a water-cooled oven and heated to 550 °C at 1200 °C/h, under an oxygen flow. At this temperature, redox cycling was started. The selectivity was determined by GC during the 10 min reduction in 4:1:1% v/v C_3H_8:C_3H_6:H_2 in Ar. The 4:1:1 ratio of reductive gases is chosen since this is the equilibrium mixture of a conventional dehydrogenation catalyst.[18] After a 4 min purge step (pure Ar), the sample was reoxidised for 18 min in 1% v/v O_2 in Ar. The redox cycle is completed by another purge step in pure Ar. The total flow rate was kept

at 50 mL min^{-1} in each step. The selectivity is determined as the ratio H_2 conversion:total conversion. Activity is determined as the percentage hydrogen combusted during the reduction step. Both selectivity and activity are averaged over eight redox cycles. The amount of coking was assessed by the amount of CO and CO_2 formed in the reoxidation step, determined by MS. All signals were normalised using a small amount of helium added to the gas feed (1 vol%), and were integrated using CasaXPS v2.1.18 software.

Procedure for TPR Experiments

TPR experiments were performed in the same set-up where catalytic activity was tested. In a typical experiment, a 250 mg sample (125–212 μm) was placed on top of a quartz wool plug in a 4 mm i.d. quartz reactor. Either 5% v/v H_2/Ar or 1% v/v C_3H_6/Ar was fed over the reactor bed, and the sample was heated from room temperature to 600 °C at 10 °C min^{-1}. The hydrogen consumption (H_2-TPR) or CO_2 evolution (C_3H_6-TPR), as determined by MS, were used to obtain the TPR profile.

Procedure for XPS Experiments

XPS was performed on a 50 mg sample. The electron analyser pass energy was 160 eV for wide scans and 40 eV for high resolution spectra. Compositions were corrected using the appropriate elemental response factors on spectra following a Shirley background subtraction.

Acknowledgements

We thank Dr. Karen Wilson (University of York) for assistance with XPS measurements, A. C. Moleman and W. F. Moolhuijzen for help with the XRD measurements, and NWO-ASPECT for financial support and feedback.

References

[1] P. C. Andrews, G. B. Deacon, C. M. Forsyth, P. C. Junk, I. Kumar, M. Maguire, *Angew. Chem.* **2006**, *118*, 5766; *Angew. Chem. Int. Ed.* **2006**, *45*, 5638.
[2] W. C. Smith, *Metals and Alloys* **1945**, *22*, 387.
[3] W. X. Dong, Y. W. Shi, Z. D. Xia, Y. P. Lei, F. Guo, *J. Electron. Mater.* **2008**, *37*, 982.
[4] R. M. Hua, *Curr. Org. Synth.* **2008**, *5*, 1.
[5] M. Rueping, B. J. Nachtsheim, W. Ieawsuwan, *Adv. Synth. Catal.* **2006**, *348*, 1033.
[6] H. Gaspard-Iloughmane, C. Le Roux, *Eur. J. Org. Chem.* **2004**, 2517.
[7] T. A. Hanna, *Coord. Chem. Rev.* **2004**, *248*, 429.
[8] J. A. Sofranko, J. J. Leonard, C. A. Jones, *J. Catal.* **1987**, *103*, 302.
[9] M. M. Bhasin, *Stud. Surf. Sci. Catal.* **1988**, *36*, 343.
[10] E. Capoen, M. C. Steil, G. Nowogrocki, M. Malys, C. Pirovano, A. Lofberg, E. Bordes-Richard, J. C. Bolvin, G. Mairesse, R. N. Vannier, *Solid State Ionics* **2006**, *177*, 483.
[11] M. C. Steil, F. Ratajczak, E. Capoen, C. Pirovano, R. N. Vannier, G. Mairesse, *Solid State Ionics* **2005**, *176*, 2305.
[12] E. Capoen, G. Nowogrocki, R. J. Chater, S. J. Skinner, J. A. Kilner, M. Mays, J. C. Boivin, G. Mairesse, R. N. Vannier, *Solid State Ionics* **2006**, *177*, 489.
[13] J. Chmielowiec, G. Paściak, P. Bujło, *J. Alloys Compd.* **2008**, *451*, 676.
[14] V. V. Kharton, F. M. B. Marques, A. Atkinson, *Solid State Ionics* **2004**, *174*, 135.
[15] A. Lofberg, S. Boujmiai, E. Capoen, M. C. Steil, C. Pirovano, R. N. Vannier, G. Mairesse, E. Bordes-Richard, *Catal. Today* **2004**, *91–92*, 79.
[16] A. Lofberg, H. Bodet, C. Pirovano, M. C. Steil, R. N. Vannier, E. Bordes-Richard, *Catal. Today* **2006**, *118*, 223.
[17] L. Ji, J. S. Liu, C. Y. Liu, X. C. Chen, *Appl. Catal. A: Gen.* **1994**, *114*, 207.
[18] R. K. Grasselli, D. L. Stern, J. G. Tsikoyiannis, *Appl. Catal. A: Gen.* **1999**, *189*, 1.
[19] J. Plotkin, E. Glatzer, *Eur. Chem. News* **2005**, *82*, 20.
[20] N. Alperowicz, *Chem. Week* **2007**, *169*, 27.
[21] N. Alperowicz, *Chem. Week* **2006**, *168*, 17.
[22] G. Parkinson, *Chem. Eng. Prog.* **2004**, *100*, 8.
[23] T. Laegreid, M. Ronnekleiv, A. Solbakken, *DGMK-conference proceedings*, **1993**.
[24] M. M. Bhasin, J. H. McCain, B. V. Vora, T. Imai, P. R. Pujado, *Appl. Catal. A: Gen.* **2001**, *221*, 397.
[25] F. Cavani, N. Ballarini, A. Cericola, *Catal. Today* **2007**, *127*, 113.
[26] R. Grabowski, *Catal. Rev. Sci. Eng.* **2006**, *48*, 199.
[27] N. R. Shiju, M. Anilkumar, S. P. Mirajkar, C. S. Gopinath, B. S. Rao, C. V. Satyanarayana, *J. Catal.* **2005**, *230*, 484.
[28] R. K. Grasselli, D. L. Stern, J. G. Tsikoyiannis, *Abstr. Pap. Am. Chem. Soc.* **1999**, *217*, U687.
[29] R. K. Grasselli, D. L. Stern, J. G. Tsikoyiannis, *Appl. Catal. A: Gen.* **1999**, *189*, 9.
[30] J. G. Tsikoyiannis, D. L. Stern, R. K. Grasselli, *J. Catal.* **1999**, *184*, 77.
[31] C. H. Lin, K. C. Lee, B. Z. Wan, *Appl. Catal. A: Gen.* **1997**, *164*, 59.
[32] L. Låte, J. I. Rundereim, E. A. Blekkan, *Appl. Catal. A: Gen.* **2004**, *262*, 53.
[33] L. Låte, W. Thelin, E. A. Blekkan, *Appl. Catal. A: Gen.* **2004**, *262*, 63.
[34] E. A. de Graaf, G. Zwanenburg, G. Rothenberg, A. Bliek, *Org. Process Res. Dev.* **2005**, *9*, 397.
[35] L. M. van der Zande, E. A. de Graaf, G. Rothenberg, *Adv. Synth. Catal.* **2002**, *344*, 884.
[36] E. A. de Graaf, A. Andreini, E. J. M. Hensen, A. Bliek, *Appl. Catal. A: Gen.* **2004**, *262*, 201.
[37] G. Rothenberg, E. A. de Graaf, A. Bliek, *Angew. Chem.* **2003**, *115*, 3488; *Angew. Chem. Int. Ed.* **2003**, *42*, 3366.
[38] J. H. Blank, J. Beckers, P. F. Collignon, F. Clerc, G. Rothenberg, *Chem. Eur. J.* **2007**, *13*, 5121.
[39] A. Trovarelli, C. de Leitenburg, M. Boaro, G. Dolcetti, *Catal. Today* **1999**, *50*, 353.
[40] J. Beckers, F. Clerc, J. H. Blank, G. Rothenberg, *Adv. Synth. Catal.* **2008**, *350*, 2237.
[41] J. Beckers, G. Rothenberg, *Dalton Trans.* **2008**, 6573.
[42] J. H. Blank, J. Beckers, P. F. Collignon, G. Rothenberg, *ChemPhysChem* **2007**, *8*, 2490.

[43] B. M. Vogelaar, J. Gast, E. M. Douma, A. D. van Langeveld, S. Eijsbouts, J. A. Moulijn, *Ind. Eng. Chem. Res.* **2007**, *46*, 421.
[44] We measured the propene conversion since the level of propane conversion is negligible.
[45] The drop in carbon deposition with increased hydrogen concentration shown in Figure 2 can also be the result of the reaction of the coke or coke precursors with the added hydrogen (J. Barbier, E. Churin, P. Marecot, *J. Catal.* **1990**, *126*, 228). The propene conversion, however, is independent of the coke formation, and also drops with increased hydrogen concentration.
[46] L. W. Lin, T. Zhang, J. L. Zang, Z. S. Xu, *Appl. Catal.* **1990**, *67*, 11.
[47] Note that part of the Pt is present as Pt(0).
[48] E. A. de Graaf, G. Rothenberg, P. J. Kooyman, A. Andreini, A. Bliek, *Appl. Catal. A: Gen.* **2005**, *278*, 187.
[49] E. B. Fox, A. F. Lee, K. Wilson, C. S. Song, *Top. Catal.* **2008**, *49*, 89.
[50] U. W. Hamm, D. Kramer, R. S. Zhai, D. M. Kolb, *Electrochim. Acta* **1998**, *43*, 2969.
[51] A. V. Tripković, K. D. Popović, R. M. Stevanović, R. Socha, A. Kowal, *Electrochem. Commun.* **2006**, *8*, 1492.
[52] V. S. Dharmadhikari, S. R. Sainkar, S. Badrinarayan, A. Goswami, *J. Electron Spectrosc. Relat. Phenom.* **1982**, *25*, 181.
[53] W. E. Morgan, W. J. Stec, J. R. V. Wazer, *Inorg. Chem.* **1973**, *12*, 953.
[54] F. M. Ismailm, Z. M. Hanafi, *Z. Phys. Chem. (Leipzig)* **1986**, *267*, 667.
[55] N. F. Dummer, R. Jenkins, X. B. Li, S. M. Bawaked, P. McMorn, A. Burrows, C. J. Kiely, R. P. K. Wells, D. J. Willock, G. J. Hutchings, *J. Catal.* **2006**, *243*, 165.
[56] F. M. Z. Zotin, L. Tournayan, J. Varloud, V. Perrichon, R. Frety, *Appl. Catal. A: Gen.* **1993**, *98*, 99.
[57] K. Sohlberg, S. T. Pantelides, S. J. Pennycook, *J. Am. Chem. Soc.* **2001**, *123*, 6609.

